Detection of Sub-20 μm Microplastic Particles by Attenuated Total Reflection Fourier Transform Infrared Spectroscopy and Comparison with Raman Spectroscopy

Ahmed M Othman, Ahmed A Elsayed, Yasser M Sabry, Diaa Khalil, Tarik Bourouina

ACS OMEGA

http://pubs.acs.org/journal/acsodf

Article

Detection of Sub-20 μm Microplastic Particles by Attenuated Total Reflection Fourier Transform Infrared Spectroscopy and Comparison with Raman Spectroscopy

Ahmed M. Othman, Ahmed A. Elsayed, Yasser M. Sabry, Diaa Khalil, and Tarik Bourouina*

Cite This: *ACS Omega* 2023, 8, 10335−10341

Read Online

ACCESS | Metrics & More | Article Recommendations | Supporting Information

ABSTRACT: Microplastics are particulate water contaminants that are raising concerns regarding their environmental and health impacts. Optical spectroscopy is the gold standard for their detection; however, it has severe limitations such as tens of hours of analysis time and spatial resolution of more than 10 μm, when targeting the production of a 2D map of the microparticle population. In this work, through a single spectrum acquisition, we aim at quickly getting information about the whole population of identical particles, their chemical nature, and their size in a range below 20 μm. To this end, we built a compact setup enabling both attenuated total reflection Fourier transform infrared (ATR-FTIR) and Raman spectroscopy measurement on the same sample for comparison purposes. We used monodisperse polystyrene and poly(methyl methacrylate) microplastic spheres of sizes ranging between 6 and 20 μm, also measured collectively using a bench-top FTIR spectrometer in ATR mode. The ATR-FTIR technique appears to be more sensitive for the smallest particles of 6 μm, while the opposite trend is observed using Raman spectroscopy. We use theoretical modeling to simulate and explain the ripples observed in the measured spectra at the shortest wavelength (higher wavenumber) region, which appears as an indicator of the microparticle dimension. The latter finding opens new perspectives for ATR-FTIR for the identification and classification of populations of nearly identical micro-scale bodies, such as bacteria and other micro-organisms, where the same measured spectrum embeds dual information about the chemical nature and the size.

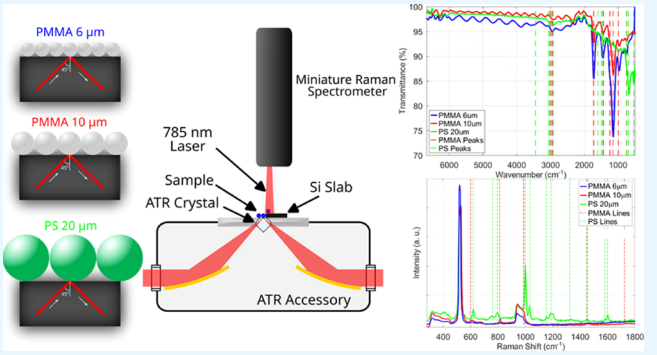

1. INTRODUCTION

Microplastic particles of various sizes and materials are known to cause pollution in aquatic and marine environments[1−4] and even in drinking water.[5] These particles could be made of polypropylene, polystyrene (PS), polyethylene, nylon, poly(methyl methacrylate) (PMMA), or poly(ethylene terephthalate),[6,7] with a size of less than 5 mm down to 1 μm[8] and many shapes such as fibers, foams, films, foils, fragments, pellets, and spheres.[9−13] Their sources in fresh water include degraded plastic waste, industrial effluents, and wastewater effluents,[14−16] while in marine environments, they arise from sources including plastic production or recycling, sandblasting, fishing gear, synthetic clothing, and packaging materials. Moreover, spherical microbeads are intentionally added to some daily consumed products including exfoliants,[17] liquid soup,[18] and toothpaste,[19] where they contribute to the microplastics found in aquatic environments.[20]

Many techniques exist in literature for the characterization of aquatic microplastics including micro-Fourier transform infrared (micro-FTIR),[21] micro-Raman,[22] attenuated total reflection FTIR (ATR-FTIR),[23,24] surface-enhanced Raman spectroscopy,[25] fluorescent material tagging,[26] flow cytometry,[27] thermogravimetric analysis,[28] and nuclear magnetic resonance.[29] However, most of these techniques require heavy sample preparation and/or are time-consuming,[30,31] especially those techniques that rely on scanning over the sample surface to produce a detailed mapping of the microplastic particles. Some techniques based on the fabrication of microfluidic chips were also developed,[31,32] where the chips were used for size sorting of the microplastics and their staining with a fluorescent material.

Many efforts were done for the purpose of comparison between these different techniques,[33−35] especially comparing the Raman and FTIR techniques for measuring of microplastics in water.[36,37] However, most of these comparisons compare Raman to FTIR microscopy (or micro-FTIR), which cannot be used for the detection of particles smaller than 10

Received: December 15, 2022
Accepted: December 28, 2022
Published: March 9, 2023

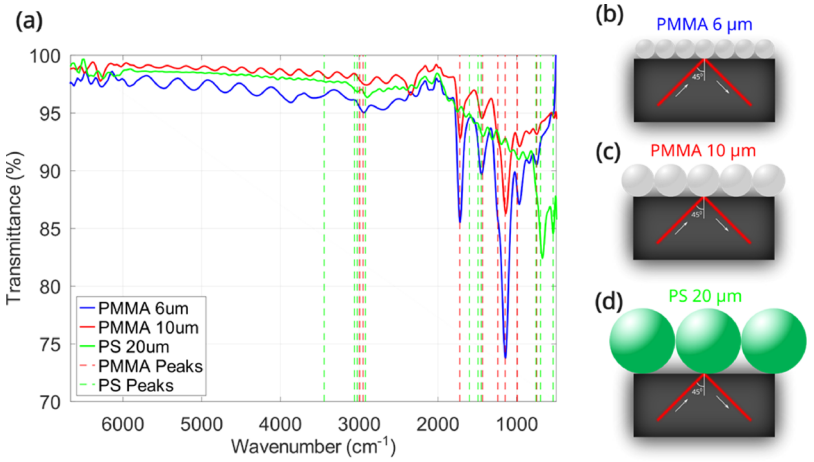

Figure 1. (a) Measured ATR transmittance spectrum for microplastic spheres using a bench-top FTIR spectrometer device. Dashed lines show the absorption peak positions for PMMA and PS. (b) PMMA 6 μm microspheres on a diamond ATR crystal, (c) PMMA 10 μm microspheres on a diamond ATR crystal, and (d) PS 20 μm microspheres on a diamond ATR crystal.

μm[38] due to the limited spatial resolution in infrared imaging. Both scanning techniques are also time-consuming, especially Raman imaging, which can accommodate much smaller spatial resolution in the order of 1 μm.

In this work, we propose a collective measurement instead of bulky and expensive spectroscopic microscopy systems, where our aim is to use compact and low-cost spectrometers for the purpose of analyzing the whole population of microplastics. Of course, by doing so we are not capturing the spatially resolved information. However, we aim to get information about both the size and material of the sample from a single spectrum. More importantly, our study revealed that through the comparison between Raman and ATR-FTIR, they could be complementary when considering different particle size ranges, where our findings show that for ATR-FTIR, smaller particles give rise to a stronger signal, which is in contrast with the Raman case where smaller particles give rise to a weaker signal.

For demonstrating the concept, we apply the technique for the identification of monodisperse PMMA and PS microplastic spheres of sizes 6, 10, and 20 μm using a bench-top FTIR-ATR spectrometer, and we simulate their FTIR-ATR spectrum in the short-wavelength (higher wavenumber) region. We also introduce a portable setup developed for measuring the microspheres using different miniaturized spectrometers and comparing their respective responses.

2. RESULTS AND DISCUSSION

2.1. Bench-Top FTIR Measurements. The transmittance spectra obtained using a bench-top FTIR setup are shown in Figure 1 for the three types of microspheres, along with the expected locations of the characteristic absorption peaks for PMMA and PS in dashed lines.[53] The measured absorbance peak wavenumbers for all spheres are shown to be in good agreement with the corresponding expected peak locations (dashed lines). Additional ripples are also found in the spectrum especially in the short-wavelength (larger wavenumber) spectral region, which can be attributed to Whispering Gallery Modes (WGM) excited inside the microspheres, which can be explained by the Mie scattering theory,[54−56] which is also known to depend on the particle dimensions.

An important observation is that the absorbance peaks of FTIR-ATR become stronger with decreasing sphere diameter, as it can be clearly seen that the PMMA 6 μm spheres have a significantly stronger absorption compared to PMMA 10 μm and the PS 20 μm showing the weakest absorption peaks. This trend can be attributed to the fact that the material fills a larger fraction of the volume containing most of the evanescent field (active region), which has an exponentially decaying optical intensity and is determined by the ATR penetration depth (d_p) above the crystal/air interface, as shown in Figure 2. The figure

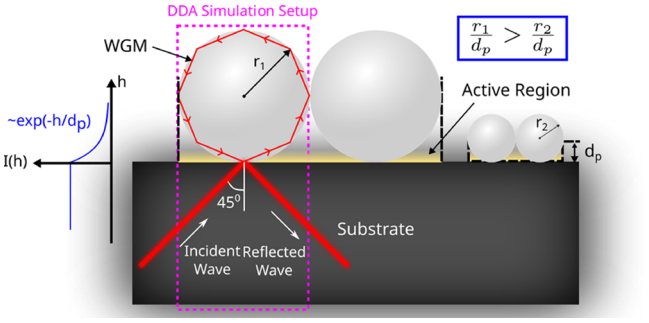

Figure 2. Illustration for the increase of the sphere fill factor for the active region in case of a small sphere compared to the case of a large sphere. The simulation setup used for DDA simulations is also shown, with arrows showing the WGM rays inside the sphere.

shows that the smaller particle size results in the spheres filling a larger fraction of the active region compared to the larger particle size, eventually resulting in a stronger absorption peak. This implies that smaller particles are easier to detect using FTIR-ATR and require a lower signal-to-noise ratio (SNR) of the spectrometer to enable easier detection and identification of the smallest particles, compared to larger particles.

It is worth mentioning at this stage that this observation suggests new perspectives for ATR-FTIR for the identification and classification of populations of identical micro-scale bodies, such as bacteria and other micro-organisms, whose dimensions are below 10 μm, where the same measured spectrum is embedding dual information about the chemical nature and the size, that is a combined bio-chemical and biophysical signature embedded in the same spectrum. For

https://doi.org/10.1021/acsomega.2c07998
ACS Omega 2023, 8, 10335−10341

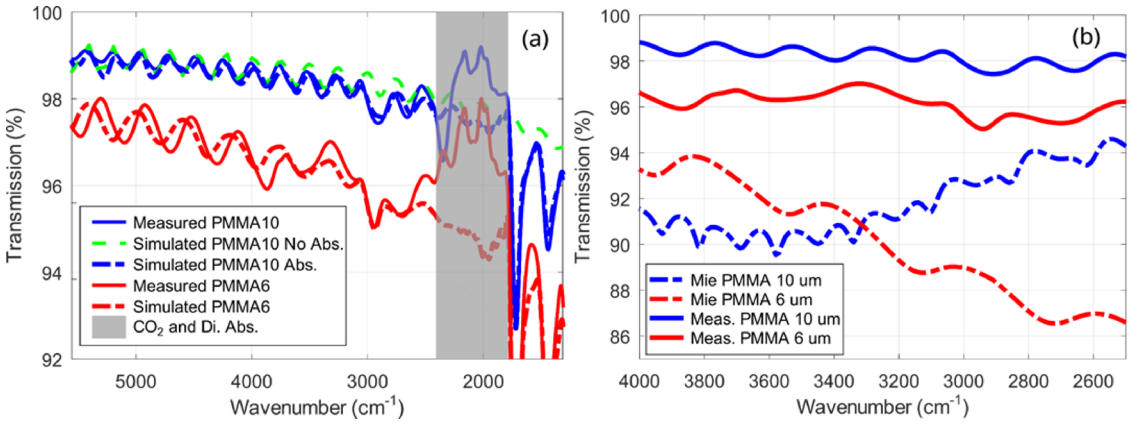

Figure 3. (a) Measured and simulated FTIR-ATR transmittance spectrum for 10 and 6 μm microplastic PMMA spheres using the DDA technique. The right part of the spectrum contains the specific absorption peak of PMMA. The central shaded region shows the region masked by CO_2 and diamond high absorption. (b) Measured FTIR-ATR transmittance spectrum for 10 and 6 μm microplastic PMMA spheres and the calculated transmittance of a single PMMA sphere using the Mie theory.

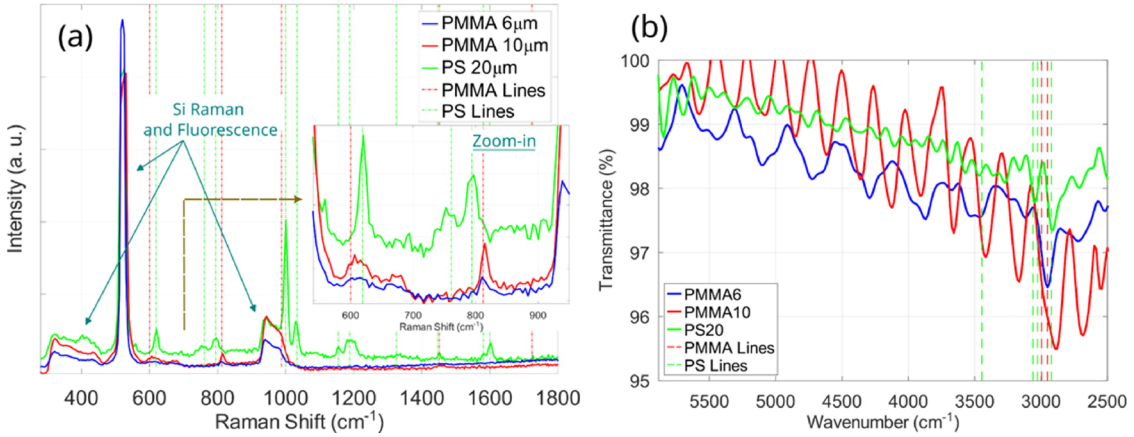

Figure 4. (a) Measured ATR transmittance spectrum for microplastic spheres using the MEMS-based miniaturized FTIR spectrometer device. Dashed lines show the absorption peak positions for PMMA and PS, with an inset showing a zoom-in view and (b) measured Raman spectrum for microplastic spheres using the miniaturized Raman spectrometer.

instance, Liu et al.[57] showed that the combination of length, diameter, and refractive index could act as a biophysical signature to identify the bacteria species. While many prior works reported on the measurement of bacteria using ATR-FTIR absorption spectra,[58,59] we propose using the ATR-FTIR spectra to retrieve their characteristic dimension embedded in the scattering ripples in order to assist, together with the absorption spectra, in identifying the bacteria species.

2.2. Microsphere ATR Simulation. In order to better explain and understand the measured spectra obtained using the FTIR-ATR spectrometer, a simulation model was developed for the different microplastic spheres under consideration in this study. The measured and simulated spectra for PMMA 10 μm and PMMA 6 μm spheres are superimposed in Figure 3a, where the simulation with non-absorbing PMMA 10 μm microspheres was also plotted for comparison. The figure shows a good agreement between the measured and simulated spectra and shows that the spectral ripples, specific to the particles dimensions, in the larger wavenumber region can be adequately explained by simulations, as shown in Figure 3a. The two absorption peaks at 2940 and 2666 cm^{-1} are also shown to be due to the specific absorption of PMMA. Some discrepancy from the simulation can be observed in the middle part of the figure (gray zone) due to the atmospheric carbon dioxide absorption present in the surrounding air, in addition to the high diamond absorption. Overall, the spectrum is showing two distinct pieces of information: (i) about the specific chemical nature of PMMA on the lower wavenumber range and (ii) about the specific size of 10 μm of those PMMA particles, in the higher wavenumber range.

In order to show that the ripples in the higher wavenumber range are caused by Mie scattering, we plot in Figure 3b the measured spectra for PMMA 10 μm and PMMA 6 μm spheres in addition to the calculated transmittance due to a single isolated sphere in space of the corresponding diameter according to Mie theory. The transmittance of the sphere T is calculated as $T = 100(1 - Q_{ext}A_{sp}/A_d)$,[60] where Q_{ext} is the extinction coefficient of a sphere using the calculated using the Mie coefficients[61] (see Supporting Information), A_{sp} is the cross-sectional area of the sphere, and A_d is the detector area, where the detector area is assumed to be 30 times the sphere area. The plot shows that the measured ripples have a similar periodicity as those resulting from the Mie theory. The Mie plots do not coincide exactly with the measurements because the experimental data are for spheres measured in ATR mode as opposed to transmission as assumed by the Mie equations.

https://doi.org/10.1021/acsomega.2c07998
ACS Omega 2023, 8, 10335−10341

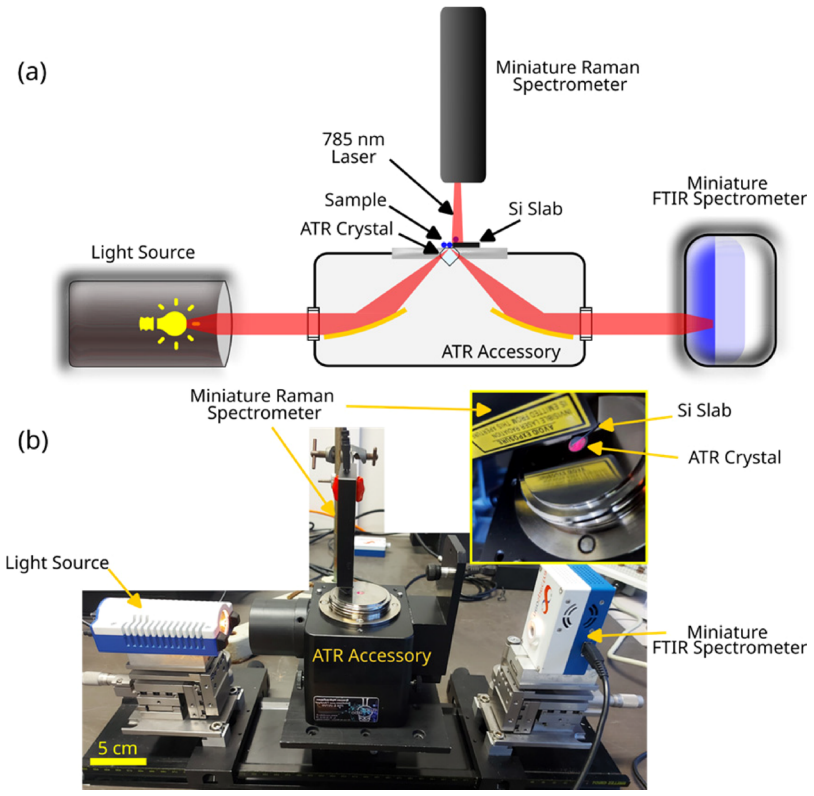

Figure 5. (a) Schematic for the miniaturized measurement setup for simultaneous measurement of microplastic spheres using ATR-FTIR and Raman spectroscopy. (b) Picture of the built setup with the inset showing a zoomed-in image of the ATR crystal with the Raman spectrometer aligned and the Si slab placed.

2.3. Miniaturized FTIR and Raman Measurements. Since ATR-FTIR appears as a suitable technique for analysis for analyzing sub-20 μm scale particles, without stringent requirements regarding the SNR, we extended our study, further considering low-cost spectrometers. To this end, we built a setup suitable for comparing two different spectrometers, whose common feature is their compactness and low cost. Both FTIR-ATR spectroscopy based on micro-electro-mechanical systems (MEMS) and a compact miniaturized Raman spectrometer were mounted together and used for the analysis of microplastic spheres. This setup has the advantages of enabling the measurement of the microplastic spheres using the FTIR and Raman spectrometers simultaneously and comparing their respective responses.

Figure 4b shows measured spectra using this setup for the different types of microspheres, where the absorption peaks can be identified, but with some difficulty due to the large Mie scattering ripples in this wavenumber range. Measured Raman spectra for different types of spheres, as well as the PMMA and PS Raman peak locations from literature,[62,63] are shown in Figure 4a, where PMMA and PS peaks can be clearly identified despite some extra peaks existing due to the silicon substrate, with good agreement with the expected peak locations. The Raman spectra were also acquired inside the water droplet before drying, with nearly the same result.

It can be clearly observed from Figure 4a that the Raman signal increases for larger particle sizes, making them easier to detect in the case of Raman spectroscopy, which is a completely opposite trend compared to FTIR-ATR spectra. This can be attributed to the small beam size of the Raman spectrometer, which detects one particle at a time. This makes the laser spectrometer beam contain more of the analyte material for larger particles, compared to smaller particles, and hence results in a larger Raman signal.

3. MATERIALS AND METHODS

3.1. Microplastic Spheres. Three types of spherical microparticles were used in the experiments, namely, PMMA microspheres of a 6 μm diameter (PMMA 6 μm), PMMA microspheres of a 10 μm diameter (PMMA 10 μm), and PS microspheres of a 20 μm diameter (PS 20 μm). The spheres were obtained from Microbeads AS, Norway.

3.2. Sample Preparation. The measurements were done on a colloidal solution of model spherical microplastic particles, of known size and chemical nature, suspended in deionized water and dispensing 50 μL of the solution using a micropipette on the top of the diamond crystal. The water was left to dry on the top of the crystal at room temperature, and the spectrum was measured after the water dried completely.

3.3. Bench-Top FTIR Measurements. The microplastic spheres were measured in ATR mode using a bench-top FTIR spectrometer (PerkinElmer Spectrum II) at a resolution of 64 cm^{-1} and a single scan with a scan time of 28 s, with a strong apodization. The spectrometer was fitted with a 3-reflection diamond ATR crystal (PIKE Miracle), which has an angle of incidence of 45^0 inside the diamond crystal, where the whole sample (all spheres) is measured in bulk without scanning. The spectrum of each reading was divided by a background spectrum, which is taken with the same setup but with no sample on the top of the diamond crystal. No correction was applied to the obtained spectra.

https://doi.org/10.1021/acsomega.2c07998
ACS Omega 2023, 8, 10335−10341

3.4. Microsphere ATR Simulation. The simulations were carried out using the discrete dipole approximation (DDA) method,[39] which approximates the scattering particle as a finite array of small polarizable dipoles and solves for the electric field in their presence, where the ADDA implementation of DDA was used.[40] This technique was chosen for its easier simulation setup compared to full electromagnetic simulation methods such as the finite-difference time domain method. The simulated setup is a wave propagating in a diamond medium and reflected at the bottom of a plastic microsphere, as shown in Figure 2, where the complex refractive index of both diamond and the plastic as functions of wavelength were taken from literature[41,42] (diamond imaginary index is neglected). The simulated spectrum was convoluted with the instrument function of the spectrometer to consider the limited spectral resolution used in the lab measurements.

3.5. Miniaturized FTIR Spectrometer. The MEMS-based FTIR spectrometer (Neospectra, Si-Ware Systems), developed by our group, uses a MEMS-based Michelson interferometer[43−46] deeply etched on a silicon substrate using the deep reactive ion etching technique,[47] a long travel range actuator,[48] and a lead selenide (PbSe) detector. This enables it to acquire spectra at a resolution of 66 cm^{-1} in the wavelength range 1350−4500 nm (wavenumber range 2500−7400 cm^{-1}), which includes only the beginning of the mid-infrared range (larger wavenumbers), in contrast to other techniques such as quantum cascade laser-based systems[49] that measure in the middle of the infrared region. A boxcar apodization function and a single scan with a scan time of 28 s were used. No correction was applied to the obtained spectra.

3.6. Miniaturized Raman Spectrometer. The Raman spectrometer (Hamamatsu Photonics C13560) uses an excitation laser at the wavelength of 785 nm with a power of 15 mW and was used to measure the microplastic spheres at a resolution of 10 cm^{-1}. The scan time was 1 s, and the number of averaged spectra was 10 for the PS 20 μm measurements and 50 for both the PMMA 6 μm and PMMA 10 μm measurements. The baseline was corrected by subtracting a linear fit from the Raman spectrum using the software provided by the spectrometer manufacturer.

3.7. Miniaturized Simultaneous FTIR and Raman Spectroscopy Setup. The same ATR accessory, as well as the same sample preparation method, were used in this setup as in the previous subsection related to the bench-top experiment. The setup, as shown in Figure 5a, includes a mid-infrared light source with a collimating lens, the ATR accessory, and the spectrometers, where the spectrometer and the light source are placed on micro-positioners to help in their optical alignment. The Raman spectrometer is placed to measure the Raman spectrum from the top, as shown in the figure. This enables the simultaneous measurement of ATR and Raman spectra. However, a problem arises in this case due to the high photoluminescence signal generated from the diamond crystal,[50,51] which saturates the Raman spectrometer. The solution used in this case was to use the tip of a silicon wafer to partially cover a small area near the diamond crystal and act as a substrate for measuring the Raman spectrum, as shown in Figure 5b, where the small silicon tip does not affect the ATR spectrum, while allowing Raman measurements to be made effectively. However, this solution is applicable for measuring homogeneous samples only and not for environmental samples that are never homogeneously distributed[52] as the ATR and the Raman spectrometers measure different parts of the sample.

The specifications of the different spectrometers used in this study are summarized in Table 1.

Table 1. Summary of the Specifications of Different Spectrometers Used

	bench-top FTIR	miniaturized FTIR	miniaturized Raman
spectral range (cm^{-1})	8300−350	6000−2300	1850−400
dimensions (cm)	46 × 30 × 23	9 × 5 × 4	7.5 × 5.5 × 1.3
resolution (cm^{-1})	66 (used for comparison) 0.5 (best)	66	10

4. CONCLUSIONS

We propose the batch analysis of microplastics using a miniaturized setup, as opposed to other time-consuming methods, which depend on measuring individual particles. Different types of plastic microparticles and sizes were measured using FTIR-ATR spectroscopy first using a bench-top FTIR spectrometer. In addition to the absorption peak that is specific to the type of plastic under consideration, the additional ripples observed in the spectrum at the lower wavelength region were attributed to Mie scattering and could serve as an indicator of the particle dimensions. The combined chemical and physical spectral signatures are adequately simulated using the DDA technique. A miniaturized portable setup was also built to simultaneously measure and compare the FTIR-ATR and the Raman spectra obtained from the different microplastic particles, with good agreement with the peaks reported in the literature. It was found that the microspheres with a smaller size give rise to a stronger FTIR-ATR signal than the larger microspheres. This is the opposite trend to the Raman signal, which is stronger for larger microspheres than smaller ones. The results of this study suggest perspectives for ATR-FTIR, which appear promising for the identification and classification of populations of identical microparticles where the same measured spectrum embeds dual information about the chemical nature and the size. Typical applications include the identification of the microbeads that are intentionally added to some daily consumed products including exfoliants,[17] liquid soup,[18] and toothpaste.[19] It can also be applied to the identification of micro-scale bodies, such as bacteria and other micro-organisms.

■ ASSOCIATED CONTENT

Supporting Information

The Supporting Information is available free of charge at https://pubs.acs.org/doi/10.1021/acsomega.2c07998.

Additional information on Mie scattering and references (PDF)

■ AUTHOR INFORMATION

Corresponding Author

Tarik Bourouina − *Université Gustave Eiffel, CNRS ESYCOM UMR 9007, Noisy-le-Grand, ESIEE, Paris 93162, France;* orcid.org/0000-0003-2342-7149; Email: tarik.bourouina@esiee.fr

https://doi.org/10.1021/acsomega.2c07998
ACS Omega 2023, 8, 10335−10341

Authors

Ahmed M. Othman − *Université Gustave Eiffel, CNRS ESYCOM UMR 9007, Noisy-le-Grand, ESIEE, Paris 93162, France; Si-Ware Systems, Cairo 11361, Egypt;* orcid.org/0000-0003-2526-1082

Ahmed A. Elsayed − *Université Gustave Eiffel, CNRS ESYCOM UMR 9007, Noisy-le-Grand, ESIEE, Paris 93162, France;* orcid.org/0000-0002-8000-2713

Yasser M. Sabry − *Si-Ware Systems, Cairo 11361, Egypt; Faculty of Engineering, Ain-Shams University, Cairo 11566, Egypt*

Diaa Khalil − *Si-Ware Systems, Cairo 11361, Egypt; Faculty of Engineering, Ain-Shams University, Cairo 11566, Egypt*

Complete contact information is available at: https://pubs.acs.org/10.1021/acsomega.2c07998

Notes

The authors declare no competing financial interest.

■ ACKNOWLEDGMENTS

This project received the support from the I-SITE FUTURE Initiative (reference ANR-16-IDEX-0003) in the frame of the project NANO-4-WATER.

■ REFERENCES

(1) Bayo, J.; Martínez, A.; Guillén, M.; Olmos, S.; Roca, M.-J.; Alcolea, A. Microbeads in Commercial Facial Cleansers: Threatening the Environment. *CLEAN − Soil, Air, Water* **2017**, *45*, 1600683.

(2) Cheung, P. K.; Fok, L. Evidence of Microbeads from Personal Care Product Contaminating the Sea. *Mar. Pollut. Bull.* **2016**, *109*, 582−585.

(3) Praveena, S. M.; Shaifuddin, S. N. M.; Akizuki, S. Exploration of Microplastics from Personal Care and Cosmetic Products and Its Estimated Emissions to Marine Environment: An Evidence from Malaysia. *Mar. Pollut. Bull.* **2018**, *136*, 135−140.

(4) Cole, M.; Lindeque, P.; Halsband, C.; Galloway, T. S. Microplastics as Contaminants in the Marine Environment: A Review. *Mar. Pollut. Bull.* **2011**, *62*, 2588−2597.

(5) Danopoulos, E.; Twiddy, M.; Rotchell, J. M. Microplastic Contamination of Drinking Water: A Systematic Review. *PLoS One* **2020**, *15*, No. e0236838.

(6) Hwang, J.; Choi, D.; Han, S.; Jung, S. Y.; Choi, J.; Hong, J. Potential Toxicity of Polystyrene Microplastic Particles. *Sci. Rep.* **2020**, *10*, 7391.

(7) Tanaka, K.; Takada, H. Microplastic Fragments and Microbeads in Digestive Tracts of Planktivorous Fish from Urban Coastal Waters. *Sci. Rep.* **2016**, *6*, 34351.

(8) Barnes, D. K. A.; Galgani, F.; Thompson, R. C.; Barlaz, M. Accumulation and Fragmentation of Plastic Debris in Global Environments. *Philos. Trans. R. Soc., B* **2009**, *364*, 1985.

(9) Pivokonsky, M.; Cermakova, L.; Novotna, K.; Peer, P.; Cajthaml, T.; Janda, V. Occurrence of Microplastics in Raw and Treated Drinking Water. *Sci. Total Environ.* **2018**, *643*, 1644−1651.

(10) Mason, S. A.; Garneau, D.; Sutton, R.; Chu, Y.; Ehmann, K.; Barnes, J.; Fink, P.; Papazissimos, D.; Rogers, D. L. Microplastic Pollution Is Widely Detected in US Municipal Wastewater Treatment Plant Effluent. *Environ. Pollut.* **2016**, *218*, 1045−1054.

(11) Su, L.; Xue, Y.; Li, L.; Yang, D.; Kolandhasamy, P.; Li, D.; Shi, H. Microplastics in Taihu Lake, China. *Environ. Pollut.* **2016**, *216*, 711−719.

(12) Anderson, P. J.; Warrack, S.; Langen, V.; Challis, J. K.; Hanson, M. L.; Rennie, M. D. Microplastic Contamination in Lake Winnipeg, Canada. *Environ. Pollut.* **2017**, *225*, 223−231.

(13) Leslie, H. A.; Brandsma, S. H.; van Velzen, M. J. M.; Vethaak, A. D. Microplastics En Route: Field Measurements in the Dutch River Delta and Amsterdam Canals, Wastewater Treatment Plants, North Sea Sediments and Biota. *Environ. Int.* **2017**, *101*, 133−142.

(14) Kirstein, I. V.; Hensel, F.; Gomiero, A.; Iordachescu, L.; Vianello, A.; Wittgren, H. B.; Vollertsen, J. Drinking Plastics? − Quantification and Qualification of Microplastics in Drinking Water Distribution Systems by MFTIR and Py-GCMS. *Water Res.* **2021**, *188*, No. 116519.

(15) Horton, A. A.; Walton, A.; Spurgeon, D. J.; Lahive, E.; Svendsen, C. Microplastics in Freshwater and Terrestrial Environments: Evaluating the Current Understanding to Identify the Knowledge Gaps and Future Research Priorities. *Sci. Total Environ.* **2017**, *586*, 127−141.

(16) Müller, A.; Österlund, H.; Marsalek, J.; Viklander, M. The Pollution Conveyed by Urban Runoff: A Review of Sources. *Sci. Total Environ.* **2020**, *709*, No. 136125.

(17) Napper, I. E.; Bakir, A.; Rowland, S. J.; Thompson, R. C. Characterisation, Quantity and Sorptive Properties of Microplastics Extracted from Cosmetics. *Mar. Pollut. Bull.* **2015**, *99*, 178−185.

(18) Gouin, T.; Roche, N.; Lohmann, R.; Hodges, G. A Thermodynamic Approach for Assessing the Environmental Exposure of Chemicals Absorbed to Microplastic. *Environ. Sci. Technol.* **2011**, *45*, 1466−1472.

(19) Carr, S. A.; Liu, J.; Tesoro, A. G. Transport and Fate of Microplastic Particles in Wastewater Treatment Plants. *Water Res.* **2016**, *91*, 174−182.

(20) Nawalage, N. S. K.; Bellanthudawa, B. K. A. Synthetic Polymers in Personal Care and Cosmetics Products (PCCPs) as a Source of Microplastic (MP) Pollution. *Mar. Pollut. Bull.* **2022**, *182*, No. 113927.

(21) Harrison, J. P.; Ojeda, J. J.; Romero-González, M. E. The Applicability of Reflectance Micro-Fourier-Transform Infrared Spectroscopy for the Detection of Synthetic Microplastics in Marine Sediments. *Sci. Total Environ.* **2012**, *416*, 455−463.

(22) Schymanski, D.; Goldbeck, C.; Humpf, H.-U.; Fürst, P. Analysis of Microplastics in Water by Micro-Raman Spectroscopy: Release of Plastic Particles from Different Packaging into Mineral Water. *Water Res.* **2018**, *129*, 154−162.

(23) Tiwari, M.; Rathod, T. D.; Ajmal, P. Y.; Bhangare, R. C.; Sahu, S. K. Distribution and Characterization of Microplastics in Beach Sand from Three Different Indian Coastal Environments. *Mar. Pollut. Bull.* **2019**, *140*, 262−273.

(24) Kunz, A.; Walther, B. A.; Löwemark, L.; Lee, Y.-C. Distribution and Quantity of Microplastic on Sandy Beaches along the Northern Coast of Taiwan. *Mar. Pollut. Bull.* **2016**, *111*, 126−135.

(25) Xu, G.; Cheng, H.; Jones, R.; Feng, Y.; Gong, K.; Li, K.; Fang, X.; Tahir, M. A.; Valev, V. K.; Zhang, L. Surface-Enhanced Raman Spectroscopy Facilitates the Detection of Microplastics <1 Mm in the Environment. *Environ. Sci. Technol.* **2020**, *54*, 15594−15603.

(26) Maes, T.; Jessop, R.; Wellner, N.; Haupt, K.; Mayes, A. G. A Rapid-Screening Approach to Detect and Quantify Microplastics Based on Fluorescent Tagging with Nile Red. *Sci. Rep.* **2017**, *7*, 44501.

(27) Kaile, N.; Lindivat, M.; Elio, J.; Thuestad, G.; Crowley, Q. G.; Hoell, I. A. Preliminary Results From Detection of Microplastics in Liquid Samples Using Flow Cytometry. *Front. Mar. Sci.* **2020**, *7*, 856.

(28) Majewsky, M.; Bitter, H.; Eiche, E.; Horn, H. Determination of Microplastic Polyethylene (PE) and Polypropylene (PP) in Environmental Samples Using Thermal Analysis (TGA-DSC). *Sci. Total Environ.* **2016**, *568*, 507−511.

(29) Peez, N.; Janiska, M.-C.; Imhof, W. The First Application of Quantitative 1H NMR Spectroscopy as a Simple and Fast Method of Identification and Quantification of Microplastic Particles (PE, PET, and PS). *Anal. Bioanal. Chem.* **2019**, *411*, 823−833.

(30) Veerasingam, S.; Ranjani, M.; Venkatachalapathy, R.; Bagaev, A.; Mukhanov, V.; Litvinyuk, D.; Mugilarasan, M.; Gurumoorthi, K.; Guganathan, L.; Aboobacker, V. M.; Vethamony, P. Contributions of Fourier Transform Infrared Spectroscopy in Microplastic Pollution Research: A Review. *Crit. Rev. Environ. Sci. Technol.* **2021**, *51*, 2681−2743.

(31) Elsayed, A. A.; Erfan, M.; Sabry, Y. M.; Dris, R.; Gaspéri, J.; Barbier, J.-S.; Marty, F.; Bouanis, F.; Luo, S.; Nguyen, B. T. T.; Liu, A.-Q.; Tassin, B.; Bourouina, T. A Microfluidic Chip Enables Fast Analysis of Water Microplastics by Optical Spectroscopy. *Sci. Rep.* **2021**, *11*, 10533.
(32) Mesquita, P.; Gong, L.; Lin, Y. A Low-Cost Microfluidic Method for Microplastics Identification: Towards Continuous Recognition. *Micromachines* **2022**, *13*, 499.
(33) Dong, M.; She, Z.; Xiong, X.; Ouyang, G.; Luo, Z. Automated Analysis of Microplastics Based on Vibrational Spectroscopy: Are We Measuring the Same Metrics? *Anal. Bioanal. Chem.* **2022**, *414*, 3359−3372.
(34) Primpke, S.; Fischer, M.; Lorenz, C.; Gerdts, G.; Scholz-Böttcher, B. M. Comparison of Pyrolysis Gas Chromatography/Mass Spectrometry and Hyperspectral FTIR Imaging Spectroscopy for the Analysis of Microplastics. *Anal. Bioanal. Chem.* **2020**, *412*, 8283−8298.
(35) Käppler, A.; Fischer, M.; Scholz-Böttcher, B. M.; Oberbeckmann, S.; Labrenz, M.; Fischer, D.; Eichhorn, K.-J.; Voit, B. Comparison of μ-ATR-FTIR Spectroscopy and Py-GCMS as Identification Tools for Microplastic Particles and Fibers Isolated from River Sediments. *Anal. Bioanal. Chem.* **2018**, *410*, 5313−5327.
(36) Cabernard, L.; Roscher, L.; Lorenz, C.; Gerdts, G.; Primpke, S. Comparison of Raman and Fourier Transform Infrared Spectroscopy for the Quantification of Microplastics in the Aquatic Environment. *Environ. Sci. Technol.* **2018**, *52*, 13279−13288.
(37) Käppler, A.; Fischer, D.; Oberbeckmann, S.; Schernewski, G.; Labrenz, M.; Eichhorn, K.-J.; Voit, B. Analysis of Environmental Microplastics by Vibrational Microspectroscopy: FTIR, Raman or Both? *Anal. Bioanal. Chem.* **2016**, *408*, 8377−8391.
(38) Shim, W. J.; Hong, S. H.; Eo, S. E. Identification Methods in Microplastic Analysis: A Review. *Anal. Methods* **2017**, *9*, 1384−1391.
(39) Hoekstra, A. G.; Sloot, P. M. A. New Computational Techniques to Simulate Light Scattering from Arbitrary Particles. *Part. Part. Syst. Charact.* **1994**, *11*, 189−193.
(40) Yurkin, M. A.; Hoekstra, A. G. The Discrete-Dipole-Approximation Code ADDA: Capabilities and Known Limitations. *J. Quant. Spectrosc. Radiat. Transfer* **2011**, *112*, 2234−2247.
(41) Zhang, X.; Qiu, J.; Zhao, J.; Li, X.; Liu, L. Complex Refractive Indices Measurements of Polymers in Infrared Bands. *J. Quant. Spectrosc. Radiat. Transfer* **2020**, *252*, No. 107063.
(42) Mildren, R. P. Intrinsic Optical Properties of Diamond. In *Optical Engineering of Diamond*; John Wiley & Sons, Ltd, 2013; pp. 1−34.
(43) Khalil, D. A.; Mortada, B.; Nabil, M.; Medhat, M.; Saadany, B. A. Compensated MEMS FTIR Spectrometer Architecture. US8531675B2 September 10, 2013.
(44) Sabry, Y. M.; Hassan, K.; Anwar, M.; Alharon, M. H.; Medhat, M.; Adib, G. A.; Dumont, R.; Saadany, B.; Khalil, D. Ultra-Compact MEMS FTIR Spectrometer. In *Next-Generation Spectroscopic Technologies X*; SPIE, 2017; Vol. *10210*, pp. 63−70.
(45) Erfan, M.; Sabry, Y. M.; Mortada, B.; Sharaf, K.; Khalil, D. Mid Infrared MEMS FTIR Spectrometer. In *MOEMS and Miniaturized Systems XV*; SPIE, 2016; Vol. *9760*, pp. 103−109.
(46) Fathy, A.; Pivert, M. L.; Kim, Y. J.; Ba, M. O.; Erfan, M.; Sabry, Y. M.; Khalil, D.; Leprince-Wang, Y.; Bourouina, T.; Gnambodoe-Capochichi, M. Continuous Monitoring of Air Purification: A Study on Volatile Organic Compounds in a Gas Cell. *Sensors* **2020**, *20*, 934.
(47) Marty, F.; Rousseau, L.; Saadany, B.; Mercier, B.; Français, O.; Mita, Y.; Bourouina, T. Advanced Etching of Silicon Based on Deep Reactive Ion Etching for Silicon High Aspect Ratio Microstructures and Three-Dimensional Micro- and Nanostructures. *Microelectron. J.* **2005**, *36*, 673−677.
(48) Medhat, M.; Nada, Y.; Mortada, B.; Saadany, B. A. Long Range Travel MEMS Actuator. US8497619B2, July 30, 2013. https://patents.google.com/patent/US8497619B2/en (accessed 2022-06-19).
(49) Primpke, S.; Godejohann, M.; Gerdts, G. Rapid Identification and Quantification of Microplastics in the Environment by Quantum Cascade Laser-Based Hyperspectral Infrared Chemical Imaging. *Environ. Sci. Technol.* **2020**, *54*, 15893.
(50) Leeds, S. M.; Davis, T. J.; May, P. W.; Pickard, C. D. O.; Ashfold, M. N. R. Use of Different Excitation Wavelengths for the Analysis of CVD Diamond by Laser Raman Spectroscopy. *Diamond Relat. Mater.* **1998**, *7*, 233−237.
(51) May, P. W.; Smith, J. A.; Rosser, K. N. 785 Nm Raman Spectroscopy of CVD Diamond Films. *Diamond Relat. Mater.* **2008**, *17*, 199−203.
(52) Thaysen, C.; Munno, K.; Hermabessiere, L.; Rochman, C. M. Towards Raman Automation for Microplastics: Developing Strategies for Particle Adhesion and Filter Subsampling. *Appl. Spectrosc.* **2020**, *74*, 976−988.
(53) Tommasini, F. J.; Ferreira, L. C.; Tienne, L. G. P.; Aguiar, V. O.; Silva, M. H. P.; Rocha, L. F. M.; Marques, M. F. V. Poly (Methyl Methacrylate)-SiC Nanocomposites Prepared through in Situ Polymerization. *Mater. Res.* **2018**, *21*, No. 20180086.
(54) Blümel, R.; Bağcioğlu, M.; Lukacs, R.; Kohler, A. Infrared Refractive Index Dispersion of Polymethyl Methacrylate Spheres from Mie Ripples in Fourier-Transform Infrared Microscopy Extinction Spectra. *J. Opt. Soc. Am. A* **2016**, *33*, 1687−1696.
(55) Shinya, A.; Fukui, M. Finite-Difference Time-Domain Analysis of the Interaction of Gaussian Evanescent Light with a Single Dielectric Sphere or Ordered Dielectric Spheres. *Opt. Rev.* **1999**, *6*, 215−223.
(56) Zambrana-Puyalto, X.; D'Ambrosio, D.; Gagliardi, G. Excitation Mechanisms of Whispering Gallery Modes with Direct Light Scattering. *Laser Photonics Rev.* **2021**, *15*, 2000528.
(57) Liu, P. Y.; Chin, L. K.; Ser, W.; Ayi, T. C.; Yap, P. H.; Bourouina, T.; Leprince-Wang, Y. An Optofluidic Imaging System to Measure the Biophysical Signature of Single Waterborne Bacteria. *Lab Chip* **2014**, *14*, 4237−4243.
(58) Castro, F. D.; Sedman, J.; Ismail, A. A.; Asadishad, B.; Tufenkji, N. Effect of Dissolved Oxygen on Two Bacterial Pathogens Examined Using ATR-FTIR Spectroscopy, Microelectrophoresis, and Potentiometric Titration. *Environ. Sci. Technol.* **2010**, *44*, 4136−4141.
(59) Parikh, S. J.; Chorover, J. ATR-FTIR Spectroscopy Reveals Bond Formation During Bacterial Adhesion to Iron Oxide. *Langmuir* **2006**, *22*, 8492−8500.
(60) Brandsrud, M. A.; Blümel, R.; Solheim, J. H.; Kohler, A. The Effect of Deformation of Absorbing Scatterers on Mie-Type Signatures in Infrared Microspectroscopy. *Sci. Rep.* **2021**, *11*, 4675.
(61) Tzarouchis, D.; Sihvola, A. Light Scattering by a Dielectric Sphere: Perspectives on the Mie Resonances. *Appl. Sci.* **2018**, *8*, 184.
(62) Mazilu, M.; Luca, A. C. D.; Riches, A.; Herrington, C. S.; Dholakia, K. Optimal Algorithm for Fluorescence Suppression of Modulated Raman Spectroscopy. *Opt. Express* **2010**, *18*, 11382−11395.
(63) Xingsheng, X.; Hai, M.; Qijing, Z.; Yunsheng, Z. Properties of Raman Spectra and Laser-Induced Birefringence in Polymethyl Methacrylate Optical Fibres. *J. Opt. A: Pure Appl. Opt.* **2002**, *4*, 237−242.

https://doi.org/10.1021/acsomega.2c07998
ACS Omega 2023, 8, 10335−10341